Archives of Mechanics • Archiwum Mechaniki Stosowanej • 26, 3, pp. 479–497, Warszawa 1974

Accelerating compressible laminar boundary layer flows of binary gas mixtures

A. WORTMAN (HAWTHORNE) and A. F. MILLS (LOS ANGELES)

COMPREHENSIVE numerical calculations have been obtained for laminar boundary layer flows of air with foreign gas injection. The injected species include H, H_2, He, Air, Xe and CCl_4 at wall cooling ratios of $g_s^* = 0.1$, 0.5 and 0.9. Values of the pressure gradient parameter β were 0 (flat plate or conical flow), 0.25, 0.5 (axisymmetric stagnation point) and 1.0 (planar stagnation point), while Mach number effects were studied by obtaining data at values of $E = u_e^2/2\mathrm{He}$ of 0, 0.5, 0.9 and 0.95. Thermodynamic properties are estimated assuming an inert ideal gas mixture and constant species specific heats; for the transport properties the rigid sphere model is used to eliminate temperature level as a problem parameter. Thermal diffusion and diffusional conduction are ignored. The effects of pressure gradient, wall cooling and Mach number on the reduction, due to mass transfer, of wall shear stress, mass transfer conductance and heat transfer rate are explained.

Otrzymano zwięzłe wyniki liczbowe, opisujące laminarne przepływy warstwy przyściennej powietrza z wtryskami obcych gazów. Wtryskiwano takie gazy jak H, H_2, He, powietrze, Xe oraz CCl_4 przy współczynnikach ochładzania ścianek $g_s^* = 0{,}1, 0{,}5$ i 0,9. Parametry gradientu ciśnienia wynosiły 0 (płytka płaska lub przepływ stożkowy), 0,25, 0,5 (osiowo-symetryczny punkt spiętrzenia) oraz 1,0 (płaski punkt spiętrzenia); zjawiska związane z liczbą Macha badano otrzymując wyniki odpowiadające wartościom $E = u_e^2/2\mathrm{H}_e$ równym 0, 0.5, 0.9 oraz 0.95. Wartości termodynamiczne oceniono przyjmując model doskonałej mieszaniny gazów szlachetnych i stałe wartości ciepła właściwego składników. Do badania własności transportu przyjęto model kulki sztywnej w celu wyeliminowania temperatury jako parametru procesu. Zaniedbano dyfuzję cieplną i przewodnictwo dyfuzyjne. Wyjaśniono wpływ gradientu ciśnienia, ochładzania ścianek oraz liczby Macha na obniżenie — w związku z transportem masy — naprężeń stycznych na ściankach, na przewodnictwo masy oraz ciepła.

Получены краткие числовые результаты, описывающие ламинарные течения пристеночного воздуха с впрысками других газов. Впрыскивались такие газы как H, H_2, He, воздух, Xe и CCl_4 при коэффициентах охлаждения стенок $g_s^* = 0.1$, 0.5 и 0.9. Параметры градиента давления равнялись 0 (плоская пластинка или коническое течение), 0.25, 0.5 (осесимметричная критическая точка), а также 1.0 (плоская критическая точка); исследовались явления связанные с числом Маха получая результаты, отвечающие значениям $E = u_e^2/2H_e$ равным 0, 0.5, 0.9 и 0.95. Термодинамические свойства оценены, принимая идеальные смеси газов и постоянные значения удельной теплоемкости компонентов. Для исследования свойств переноса принята модель жесткого шарика с целью исключения температуры как параметра процесса. Пренебрегалось термодиффузией и диффузной проводимостью. Выяснено влияние градиента давления, охлаждения стенок и числа Маха на снижение — в связи с переносом массы — касательных напряжений на стенках и на перенос массы и тепла.

Nomenclature

C $\varrho\mu/(\varrho\mu)_e$,

C_f $2\tau_s/\varrho u_e^2$, skin friction coefficient,

C_p specific heat,

$\mathscr{D}$ binary diffusion coefficient,

E $u_e^2/2\mathrm{H}_e$, kinetic energy or Mach number parameter,

f dimensionless stream function such that $f' = u/u_e$
g enthalpy ratio H/H_e; conductance,
g_h $q_s/C_{pe}(T_r - T_s)$, heat transfer conductance,
$g_{m,i}$ $j_{i,s}/(m_{i,s} - m_{i,e})$, mass transfer conductance,
h enthalpy,
H total enthalpy,
j species diffusive flux,
k thermal conductivity,
Le $\varrho C_p \mathscr{D}/k$, Lewis number,
M molecular weight,
m mass fraction,
$\dot{m}$ mass transfer rate,
N_{Av} Avogadro's number,
P pressure,
Pr $C_p\mu/k$, Prandtl number,
q conductive heat flux,
$\mathscr{R}$ universal gas constant,
r recovery factor; also radius of an axisymmetric surface,
s, y streamwise and normal coordinates, respectively,
Sc $\mu/\varrho\mathscr{D}$, Schmidt number,
T absolute temperature,
u, v velocity components,
z_1 $m_1/m_{1,s}$, normalized mass fraction,
β^0 $dlnu_e/dln\xi$,
β $\beta^0/(1-E)$, pressure gradient or acceleration parameter,
ε geometrical index,
η transformed coordinate normal to the surface, equation (2.7),
μ dynamic viscosity,
ϱ density,
σ collision diameter,
ξ transformed coordinate along the surface, equation (2.8),
τ shear stress,
ψ stream function,

Subscripts

e free stream,
f friction,
es gas of free stream composition at surface temperature,
h heat transfer,
i, j species i and j,
m mass transfer,
o reservoir,
r recovery,
s surface (wall),
1, 2 injected and free stream species, respectively.

Superscripts

$'$ differentiation with respect to η,
$*$ zero mass transfer.

1. Introduction

COMMENCING with the pioneering work of BARON in 1956 [1], there have been numerous studies of the effects of mass transfer on compressible laminar boundary layer flows of binary gas mixtures. Of primary interest has been the reduction of the wall shear stress, the mass transfer conductance and the heat transfer rate. Such studies are of fundamental importance to the theory of laminar boundary layers; also the results find engineering application for the prediction of transpiration, evaporation and sublimation processes. The work prior to 1960 has been reviewed by GROSS *et al.* [2]. For self-similar zero pressure gradient flows, results obtained prior to 1968 were correlated by SIMON, HARTNETT and LIU [3, 4]. For stagnation point flows the more significant work is that of SPARROW *et al.* [5], LIBBY and SEPRI [6], ANFIMOV [7], GOMEZ *et al.* [8] and MILLS and WORTMAN [9]. In order to reduce the computational task, each study has covered a limited range of the pertinent parameters, such as pressure gradient, Mach number and temperature ratio. Also, difference in the detailed manner in which thermodynamic and transport properties were modeled precludes a meaningful compilation of the available data. As a result, the effects of the various problem parameters on the wall shear stress, the mass transfer conductance and the heat transfer rate, are not easily evaluated. There is indicated a need for a set of data which spans the relevant parameters in a more comprehensive manner.

We view self-similar solutions of the laminar boundary layer equations as having a number of uses. Firstly, the solutions may exactly represent the interesting physical situation, for example, at stagnation points. Secondly, self-similar solutions have practical utility when used in conjunction with the assumption of local similarity to calculate general boundary layer flows. Though, in this context, the recent work of JAFFE *et al.* [10], KENDALL and BARTLETT [11], and DENNY and KOCHAN [12], has shown that direct solution of the governing partial differential equations is quite feasible for the practical calculation of nonsimilar flows with mass transfer. Thirdly, self-similar solutions conveniently exhibit the effects of the various flow parameters, namely: pressure gradient, Mach number, wall to free stream temperature ratio, gas property variations and mass transfer rate. It is to this last mentioned purpose that the present paper is primarily directed. Our calculations have spanned a wide range of the parameters; the intent is to display the results in a manner which allows the effect of the parameters to be readily discerned.

2. Analysis

The coordinate system is so chosen that s is measured along and y perpendicular to the surface; the corresponding velocity components are u and v, respectively. For steady laminar boundary layer flow of a binary gas mixture, the governing conservation equations are:

mass

$$\frac{\partial}{\partial s}(\varrho u r^{\varepsilon})+\frac{\partial}{\partial y}(\varrho v r^{\varepsilon}) = 0; \tag{2.1}$$

momentum

$$\varrho u\frac{\partial u}{\partial s}+\varrho v\frac{\partial u}{\partial y} = -\frac{\partial p}{\partial s}+\frac{\partial}{\partial y}\left(\mu\frac{\partial u}{\partial y}\right); \tag{2.2}$$

species

$$\varrho u\frac{\partial m_1}{\partial s}+\varrho v\frac{\partial m_1}{\partial y} = \frac{\partial}{\partial y}\left(\varrho\mathscr{D}_{12}\frac{\partial m_1}{\partial y}\right); \tag{2.3}$$

total enthalpy

$$\varrho u\frac{\partial H}{\partial s}+\varrho v\frac{\partial H}{\partial y}=\frac{\partial}{\partial y}\left(k\frac{\partial T}{\partial y}+\varrho\mathscr{D}_{12}\frac{\partial m_1}{\partial y}(h_1-h_2)\right)+\frac{\partial}{\partial y}\left(\mu u\frac{\partial u}{\partial y}\right). \tag{2.4}$$

The geometrical index ε assumes a value of 1 for an axisymmetric flow and 0 for a planar one. Second-order boundary layer effects, such as transverse curvature, are ignored. Also, thermal diffusion and diffusional conduction are neglected; these phenomena are unimportant for the cooled wall situations emphasized in the present study [5, 9, 13]. The boundary conditions imposed on the set of equations are

$$y = 0: u = 0,$$

$$\varrho v = \dot{m}, \tag{2.5}$$

$$\dot{m} = m_{1,s}\dot{m}-\varrho\mathscr{D}_{12}\frac{\partial m_1}{\partial y}\bigg|_s;$$

$$T = T_s;$$

$$y \to \infty: u \to u_e,$$

$$m_1 \to 0, \tag{2.6}$$

$$\mathrm{H} \to H_e.$$

Following LEES [14], the transformation $s, y \to \xi, \eta$ is made where the Levy and Mangler transformations have been combined in defining

$$\eta = \frac{\varrho_e u_e}{(2\xi)^{1/2}}\int_0^y r^\varepsilon\frac{\varrho}{\varrho_e}dy, \tag{2.7}$$

$$\xi = \int_0^s \varrho_e\mu_e u_e r^{2\varepsilon}ds. \tag{2.8}$$

A stream function ψ is introduced such that

$$\varrho u r^\varepsilon = \frac{\partial\psi}{\partial y}, \quad \varrho v r^\varepsilon = -\frac{\partial\psi}{\partial s} \tag{2.9}$$

and choosing $\psi(\xi, \eta) = (2\xi)^{1/2}f(\eta)$ leads to

$$\frac{u}{u_e} = \frac{\partial f}{\partial\eta} = f'. \tag{2.10}$$

Under this transformation the governing equations for self-similar flows are, in non-dimensional form,

$$(Cf'')'+ff'' = \beta^0\left(f'^2-\frac{\varrho_e}{\varrho}\right), \tag{2.11}$$

$$\left(\frac{C}{Sc}z_1'\right)'+fz_1' = 0, \tag{2.12}$$

$$\left(\frac{C}{Pr}g'\right)'+fg' = E\left[2C\left(\frac{1}{Pr}-1\right)f'f''\right]'+\left[\frac{C}{Sc}(g_1-g_2)\left(\frac{1}{Le}-1\right)m_{1,s}z_1'\right]', \tag{2.13}$$

which are to be solved subject to

$$\eta = 0: \quad f = f_s;\ f' = 0;\ m_{1,s} = \left.\frac{f}{f+\frac{C}{Sc}z_1'}\right|_s;\ g = g_s^*, \tag{2.14}$$

$$\eta \to \infty: \quad f' \to 1;\ z_1 \to 0;\ g \to 0. \tag{2.15}$$

2.1. Thermodynamics and transport properties

The thermodynamic and transport properties of mixture were computed assuming an ideal gas mixture and constant species specific heats. The species viscosity, thermal conductivity and binary diffusion coefficients were computed assuming a rigid sphere molecular interaction model, viz.,

$$\mu_i = \frac{5}{16}\left(\frac{\mathscr{R}TM_i}{\pi}\right)^{1/2}\frac{1}{N_{Av}\sigma_i^2},$$

$$k_i = \mu_i\left(C_{pi}+\frac{5}{2}\frac{\mathscr{R}}{M_i}\right), \tag{2.16}$$

$$\varrho\mathscr{D}_{ij} = \frac{3}{8}\left(\frac{\mathscr{R}T}{\pi}\right)^{1/2}\left(\frac{M_i+M_j}{2M_iM_j}\right)\frac{M}{N_{Av}\left(\frac{\sigma_i+\sigma_j}{2}\right)^2}$$

and the mixture rules are, from Ref. [15],

$$\mu = \sum_{j=1}^{2}\frac{x_j\mu_j}{\sum_{k=1}^{2}x_jG_{jk}}; \quad k = \sum_{j=1}^{2}\frac{x_jk_j}{\sum_{k=1}^{2}x_jG_{jk}},$$

where

$$G_{jk} = 1.154\left(\frac{1+\sigma_k/\sigma_j}{2}\right)^2\left(\frac{2}{M_j/M_k+1}\right)^2, \quad j \neq k$$

$$= 1.0 \qquad\qquad\qquad\qquad\qquad\qquad\qquad\qquad j = k.$$

Table 1. Thermodynamic and transport properties of the injecteed gases

Species	M	$\frac{M}{M_{air}}$	$\frac{\sigma}{\sigma_{air}}$	$\frac{C_p}{C_{p\,air}}$	$\frac{\mu}{\mu_{air}}$	$\frac{k}{k_{air}}$	Sc_e
H	1.008	0.03480	0,7410	20.48	0.340	7.693	0.164
H_2	2.016	0.06959	0.8059	14.21	0.460	5.786	0.245
He	4.004	0.1382	0.7122	5.156	0.733	4.177	0.301
Air	28.97	1.000	1.000	1.00	1.000	1.000	0.833
Xe	131.3	4.532	1.121	0.1570	1.694	0.294	1.200
CCl_4	153.8	5.309	1.651	0.5378	0.845	0.377	1.900

The molecular weights, collision cross-sections and specific heats were obtained from Refs. [16, 6, and 17] and are listed in Table 1. In estimating properties in this manner our objective was to eliminate temperature level as a problem parameter; the transport properties, when normalized by free stream values, are functions of temperature ratio T/T_e, and injectant concentration only.

2.2. Solution Procedure

The calculation method used in the present study was developed in Ref. [10], where it was applied to a wide range of boundary layer problems. The method is an iterative one, with special care taken to ensure establishment of a converging sequence of successive iterates. Computer time (IBM 360/75 system) was typically 4 seconds per solution for four place accuracy. Detailed discussion of the method may be found in Refs. [18 and 19], where accuracy and reliability are demonstrated for several different classes of problem.

3. Results and discussion

The situations computed were as follows. For zero pressure gradient flows ($\beta = 0$), the injectants were: H, H_2, He, Air, Xe and CCl_4, with $E = 0$, 0.5, 0.9, 0.95. For $\beta = 0.25$, the injectants were He, Air and Xe, with $E = 0$, 0.5, 0.9, 0.95; for $\beta = 0.5$, He, Air and Xe with $E = 0$, 0.5, 0.9; and for $\beta = 1.0$, He, Air and Xe with $E = 0$. For all cases, three values of the enthalpy ratio $g_s^* = h_{es}/H_e$ were considered: 0.1, 0.5, 0.9. In all, over 1500 solutions were obtained. In Ref. [18] can be found complete tabulations of the quantities

(i) the wall shear stress function $C_s f_s''$;
(ii) the wall conduction heat flux function $C_s g_s'/Pr_s$;
(iii) the mass transfer conductance function $C_s z_s'/Sc_s$;
(iv) the wall value of the injectant concentration $m_{1,s}$;
(v) the wall value of $\varrho\mu/(\varrho\mu)_e = C_s$;
(vi) the wall value of the Prandtl number Pr_s;
(vii) the wall value of the Schmidt number Sc_s.

Table 2 contains a selection of data; these data might be useful to other workers for evaluation of accuracy and reliability.

Table 2. Data for selected cases: complete tabulations may be found in Ref. 18

Injectant	β	E	g_s	$-f_s$	$C_s f_s''$	$\frac{C_s}{Pr_s} g_s'$	$-\frac{C_s}{Sc_s} z_s'$	C_s	Pr_s	Sc_s
H_2	0	0	0.1	0	0.5707	0.6158	1.3526	3.1623	0.7402	0.2451
H_2	0	0	0.1	0.3	0.0422	0.1199	0.0382	0.1044	0.6994	1.3380
H_2	0	0.9	0.5	0 1	0.0894	0.0258	0.1409	0.0385	0.5340	0.9057
H	0	0	0.1	0.05	0.4381	0.6541	1.0770	1.2698	0.3376	0.3271
H	0	0.95	0.5	0.05	0.1046	0.0172	0.2114	0.0326	0.3668	0.6711
He	0	0	0.5	0.2	0.2115	0.1914	0.3287	0.3540	0.5106	0.8497
He	0	0.5	0.5	0.1	0.2947	0.1662	0.5518	0.4699	0.5061	0.5415
He	0	0.9	0.1	0.1	0.2438	0.2495	0.4500	0.4253	0.5000	0.5826
Xe	0		0.5	0.5	0.2967	0.2122	0.3271	3.3076	0.6032	0.7849
CCl_4	0	0.5	0.5	0.5	0.2165	0.1247	0.2131	2.0797	0.6837	0.7337
He	0.25	0	0.1	0.3	0.3187	0.3803	0.3100	0.6234	0.5346	1.0012
He	0.25	0.5	0.1	0.1	0.4774	0.4513	0.7467	1.2048	0.5199	0.4890
Xe	0.25	0.5	0.5	1.0	0.2744	0.0927	0.2214	3.9241	0.5838	0.6166
He	0.5	0.5	0.1	0.5	0.2003	0.1130	0.0518	0.2500	0.6423	1.4833
He	0.5	0.9	0.1	0.2	0.2652	0.1796	0.2694	0.2264	0.5194	0.9113
He	0.5	0.5	0.5	0.8	0.4558	0.1276	0.2871	3.1360	0.5862	0.6842
He	1.0	0	0.5	1.0	0.4960	0.0208	0.0011	0.1434	0.6690	1.5948
He	1.0	0	0.9	2.0	0.6219	0.0194	0.1834	5.6993	0.6008	0.5307

3.1. Effects of injected species

Figures 1a, 1b and 1c show the shear stress $\tau_s = \mu\,\partial\mu/\partial y|_s$, mass transfer conductance $g_m = j_{1,s}/(m_{1,s}-m_{1,e})$, and heat transfer rate $q_s = -k\,\partial T/\partial y|_s$, each normalized by their respective zero mass addition values, for zero pressure gradient flows under "cold wall" conditions ($g_s = 0.1$), and at moderate Mach number ($E = 0.5$). The important features of the data may be explained using the assessment of binary boundary layer flows given in Refs. [8 and 13], where a wide variety of injectants were considered. Briefly the

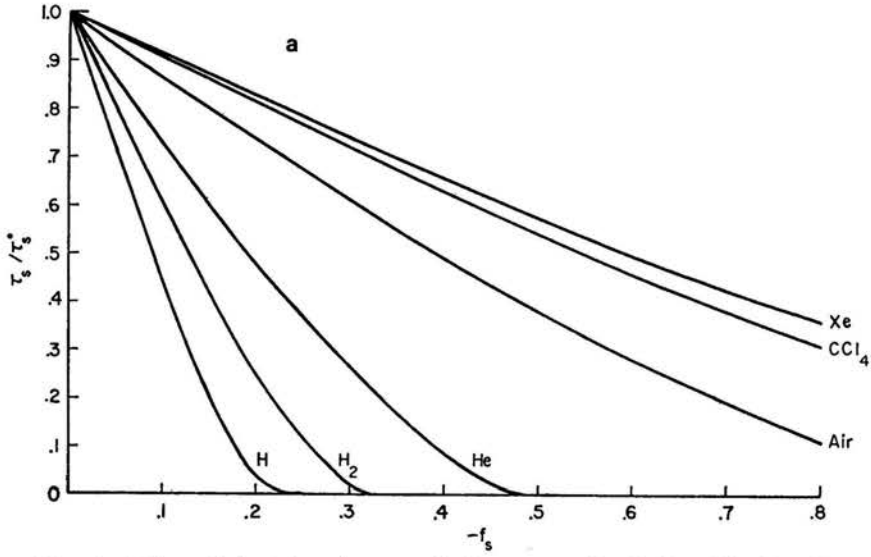

FIG. 1a. Effect of injected species on wall shear stress. $\beta = 0$, $E = 0.5$, $g_s^* = 0.1$.

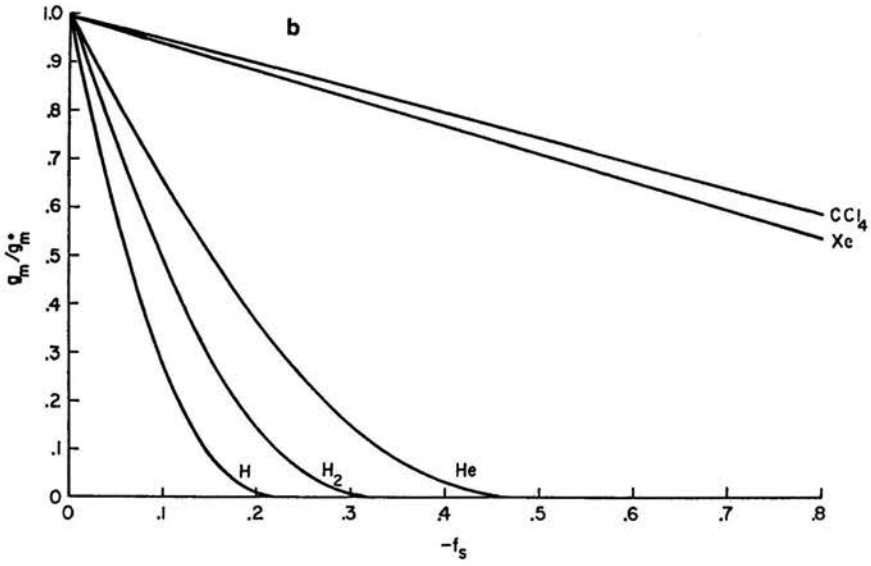

FIG. 1b. Effect of injected species on mass transfer conductance. $\beta = 0$, $E = 0.5$, $g_s^* = 0.1$.

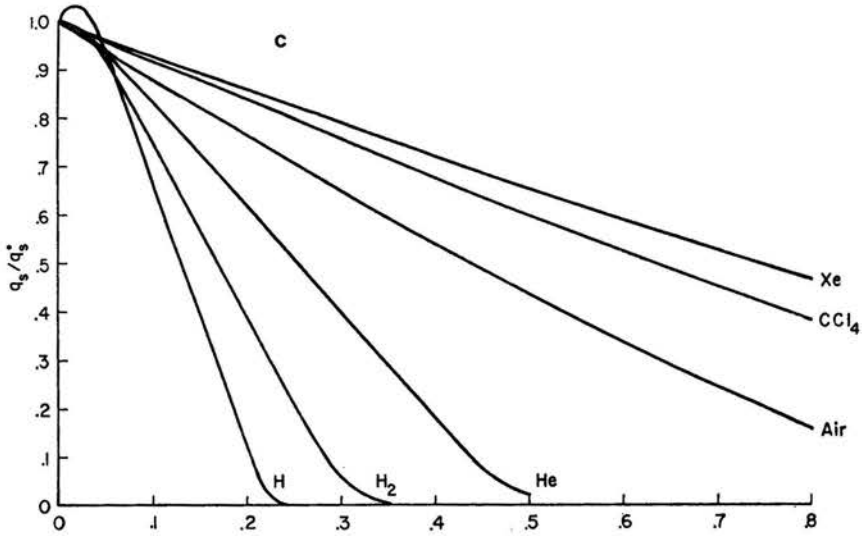

FIG. 1c. Effect of injected species on heat transfer rate. $\beta = 0$, $E = 0.5$, $g_s^* = 0.1$.

arguments are as follows: There is a primary properties variation influenced through $C = (\varrho\mu)/(\varrho\mu)_e$ on momentum, species and energy transport; the dependence is approximately as $C_s^{0.1}$ at low injection rates, with the exponent increasing as injection distorts the concentration profile. Viscosity variations are significant only for the light injectants; for heavy injectants the effect of C is essentially a density effect. In addition, (i) the mass transfer conductance is strongly influenced through variations in the Schmidt number, which particularly for heavy injectants, is essentially a density effect, and (ii) the heat transfer rate is strongly influenced through variations in the Prandtl number which, except at low injection rates of H, H_2 and He, is essentially a specific heat effect.

The data presented in Figs. 1a, 1b and 1c for $\beta = 0$ exhibit features already noted for axisymmetric stagnation points ($\beta = 0.5$) in Ref. [9]. For example: (i) CCl_4 is more effective than Xe in reducing shear stress, due to its markedly lower viscosity, (ii) the effectiveness of the injectants in reducing the mass transfer conductance behaves quite regularly with molecular weight, (iii) the anomalous behavior of heat transfer for H, H_2 and He at low injection rates, due to an increased thermal conductivity near the wall, is clearly shown in Fig. 1c, and (iv) CCl_4 is more effective than Xe in reducing heat transfer due to its higher specific heat. For further discussion of the effects of injected species the reader is referred to Ref. [9].

3.2. Effects of pressure gradient

Figures 2a, 2b and 2c show the effects of pressure gradient on the shear stress, mass transfer conductance and heat transfer rate, respectively. The data presented is for $E = 0$ at $g_s^* = 0.1$, i.e., low speed, cold wall, flows. The ratios τ_s/τ_s^*, g_m/g_m^* and q_s/q_s^*

all increase with increasing β. The effect of the pressure gradient is to accelerate the flow and an increase in the wall fluxes results, as can be most easily seen for the shear stress by examining Eq. (2.11). Normalization with the zero mass transfer values does not completely remove the dependence on β owing to the distortion of the velocity and $(\varrho\mu)$ profiles by mass transfer. A comparison of Figs. 2a, 2b and 2c shows that the effect of β is most marked for shear stress, as would be expected from the direct manner in which the pressure gradient enters the momentum balance.

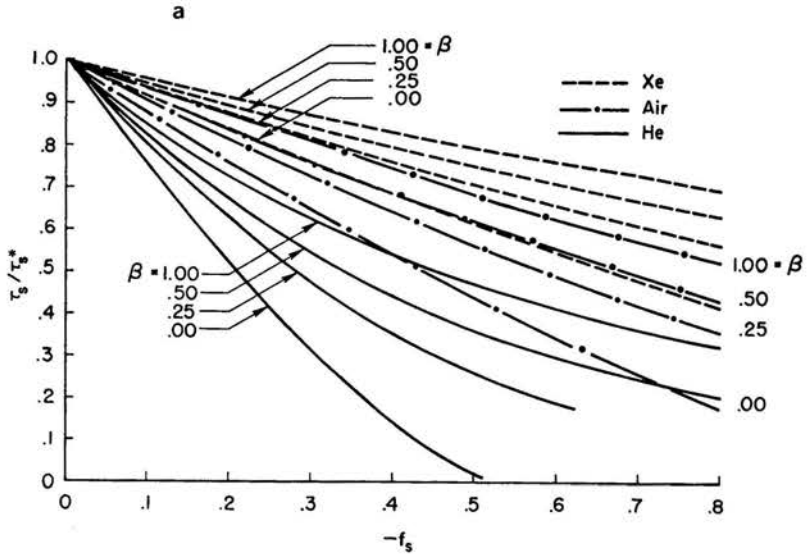

FIG. 2a. Effect of pressure gradient on wall shear stress. $E = 0$, $g_s^* = 0.1$.

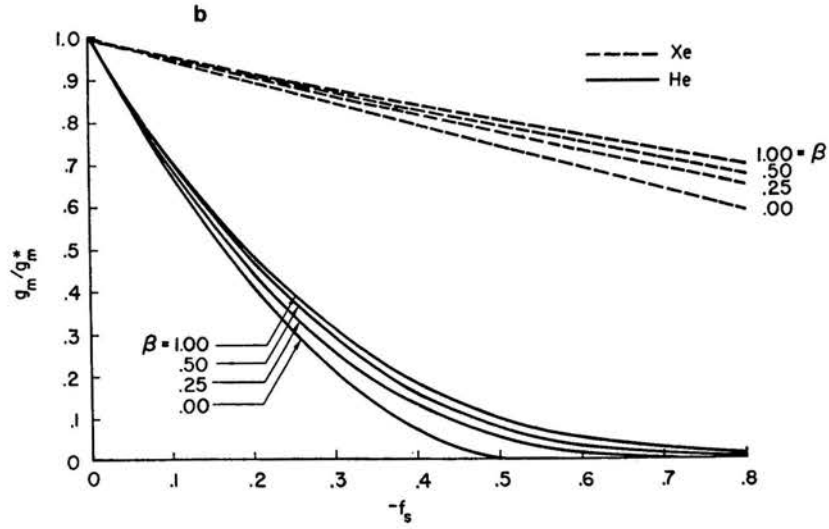

FIG. 2b. Effect of pressure gradient on mass transfer conductance. $E = 0$, $g_s^* = 0.1$.

The cold wall ($g_s^* = 0.1$) for the data in Figs. 2 minimizes the effect of β. Recall the "heavy surface layer" approximation of LEES [14] where it was demonstrated that the pressure gradient term in the momentum conservation equation, $\beta^0(f'^2 - \varrho_e/\varrho)$, becomes

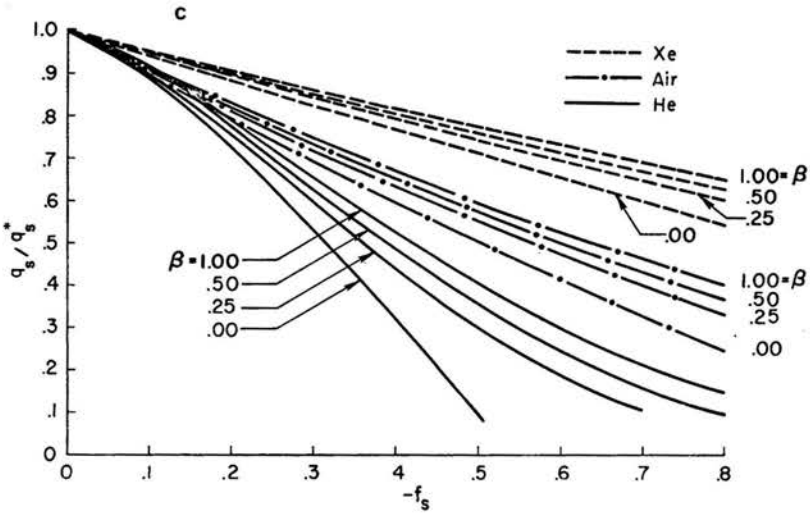

FIG. 2c. Effect of pressure gradient on heat transfer rate. $E = 0$, $g_s^* = 0.1$.

small as $g_s \to 0$. For $g_s = 0$, ϱ_e/ϱ varies from 0 to 1 across the boundary layer, as does f', and a net cancellation tends to result. With foreign gas injection, the degree to which the heavy surface layer limit is approached is markedly dependent on the injectant molecular weight. Thus β has its greatest effect for light injectants at high wall temperatures.

Associated with the above mentioned phenomena is the behavior at high blowing rates. For $\beta \leqslant 0$ boundary layer "blow-off", i.e., zero wall shear stress, occurs at a definite value of $-f_s$; for $\beta > 0$, the shear stress decreases with increasing $-f_s$, but never becomes identically zero. Boundary layer separation on an impermeable wall and boundary layer blow-off are analogous. Boundary layer separation on an impermeable wall occurs for negative β due to the adverse pressure gradient decelerating fluid near the wall. Similarly, for flows with mass transfer, a favorable pressure gradient ($\beta > 0$) accelerates fluid near the wall and must act to delay apparent blow-off. Finally, since most of the essential features of the effect of pressure gradient are exhibited by the data for air injection, the reader is referred to Ref. [19] for data and a discussion of the effects of like gas injection in the range $0 \leqslant \beta \leqslant 20$.

3.3. Effects of wall cooling

Figures 3 and 4 show, for $E = 0$ and 0.9 respectively, the effects of wall cooling on the reduction in shear stress, mass transfer conductance and heat transfer, for flows with $\beta = 0$. In the absence of a pressure gradient the enthalpy ratio $g_s^* = h_{es}/H_e$ enters the problem

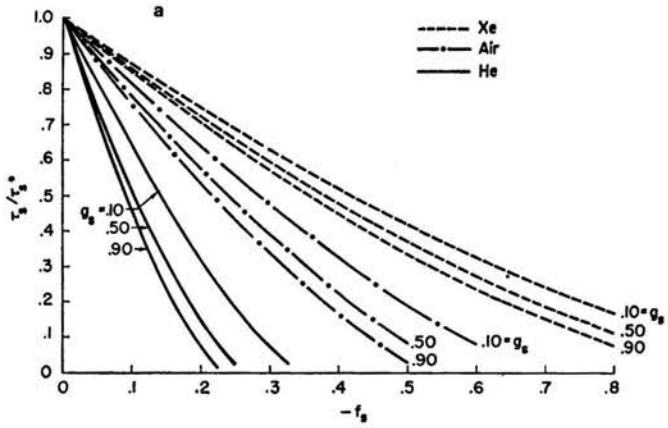

FIG. 3a. Effect of wall cooling on wall shear stress. $\beta = 0$, $E = 0$.

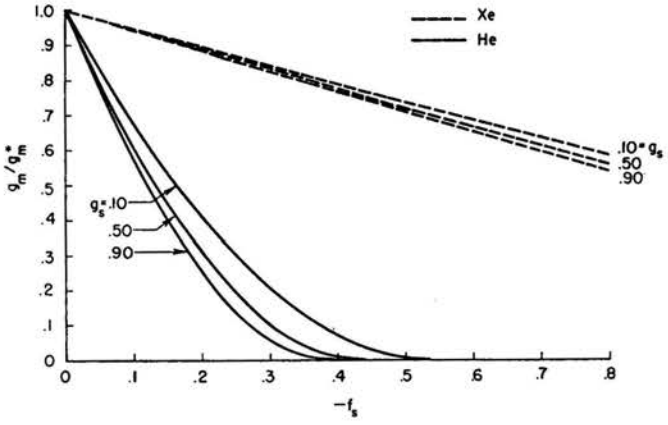

FIG. 3b. Effect of wall cooling on mass transfer conductance. $\beta = 0$, $E = 0$.

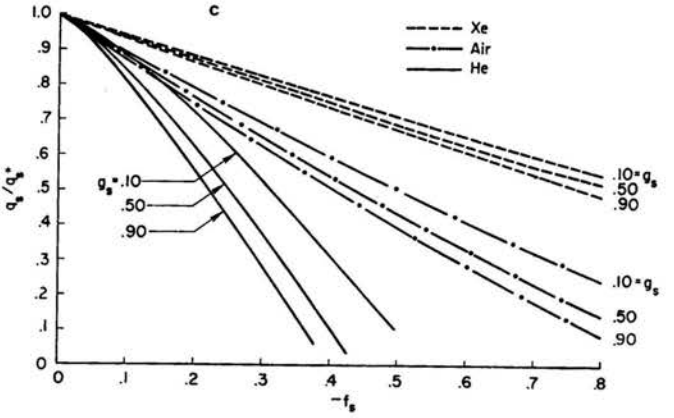

FIG. 3c. Effect of wall cooling on heat transfer rate. $\beta = 0$, $E = 0$.

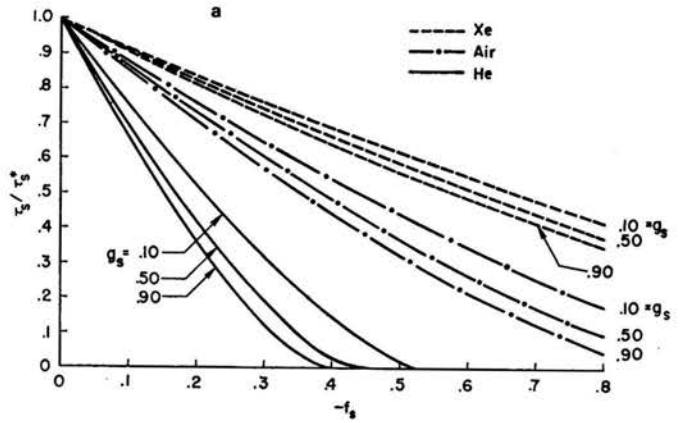

FIG. 4a. Effect of wall cooling on wall shear stress. $\beta = 0$, $E = 0.9$.

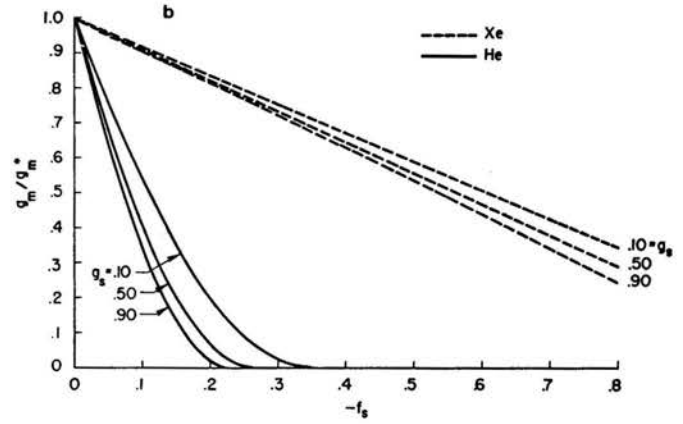

FIG. 4b. Effect of wall cooling on mass transfer conductance. $\beta = 0$, $E = 0.9$.

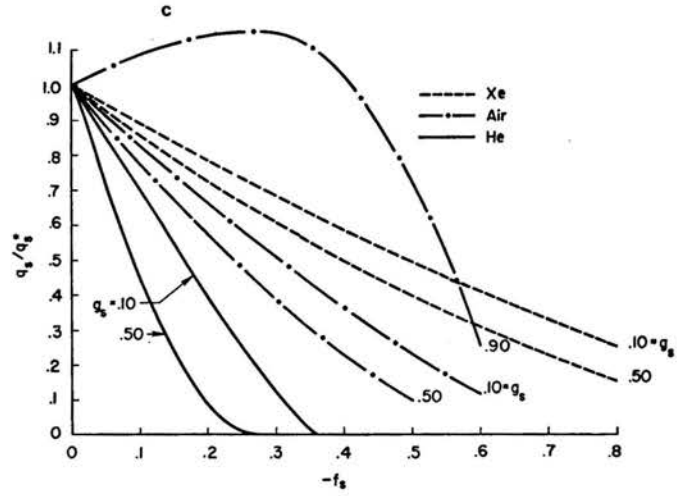

FIG. 4c. Effect of wall cooling on heat transfer rate. $\beta = 0$, $E = 0.9$.

through the variation of $C = (\varrho\mu)/(\varrho\mu)_e$ across the flow. Increased wall temperatures lead to decreased values of C_s and hence decreases in τ_s, g_m and q_s. Normalization with zero mass transfer values does not completely remove the effect of g_s^* due to the distortion of the C profile by mass transfer; the flattening of the profile near wall extends the influence of the wall value of C further into the boundary layer. The data in Figs. 3 and 4 support the above evaluation, with the exception of heat transfer at $g_s^* = 0.9$ in Fig. 4c. But this anomaly is due to viscous dissipation at the high value of $E(0.9)$, and will therefore be discussed in the following section.

When a pressure gradient is present, the resulting acceleration is sufficient to reverse the trend described above for the shear stress; even at $\beta = 0.25$, τ_s and τ_s/τ_s^* increase with increasing wall temperature owing to the first-order effect of the pressure gradient in the momentum equation. On the other hand, both g_m/g_m^* and q_s/q_s^* decrease with increasing wall temperature, even at $\beta = 0.1$; however, the decreases become less marked at higher β. Thus it is apparent that the effect of temperature ratio on C dominates the behavior of the species and energy equations, with only a secondary effect of the flow acceleration being felt through the density ratio.

3.4. Effect of Mach number

The parameter $E = u_e^2/2H_e$ is a measure of the kinetic energy available for conversion into thermal energy within the boundary layer. For flow over a flat plate, E may be expressed in terms of the Mach number of the free stream, but in so doing, a value of the adiabatic exponent γ must be introduced. For hypersonic flow over a cone, the assumption of

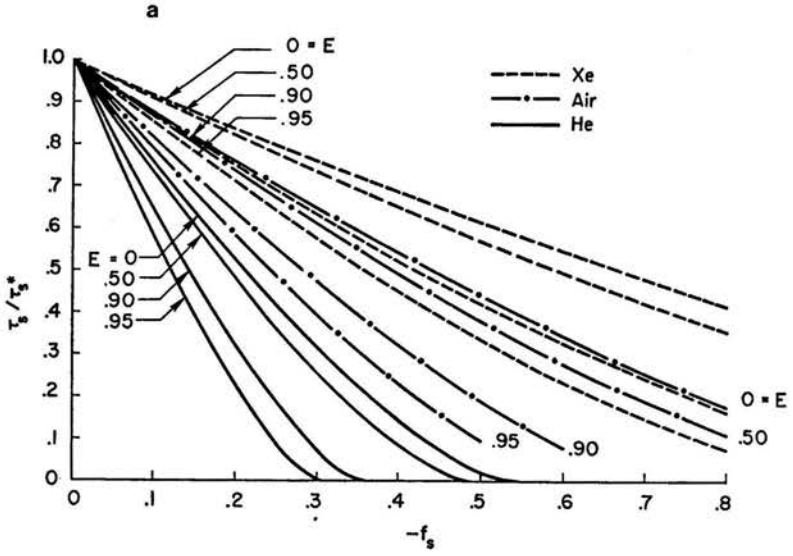

FIG. 5a. Effect of Mach number on wall shear stress. $\beta = 0$, $g_s^* = 0.1$.

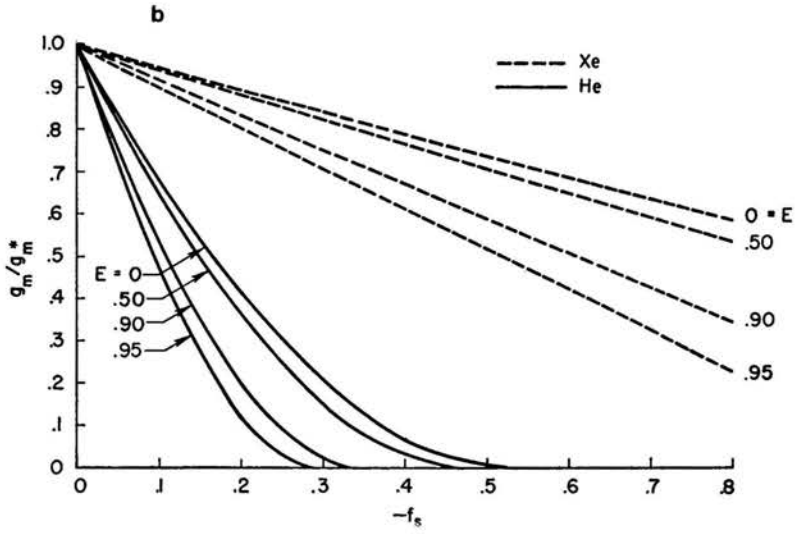

FIG. 5b. Effect of Mach number on mass transfer conductance. $\beta = 0$, $g_s^* = 0.1$.

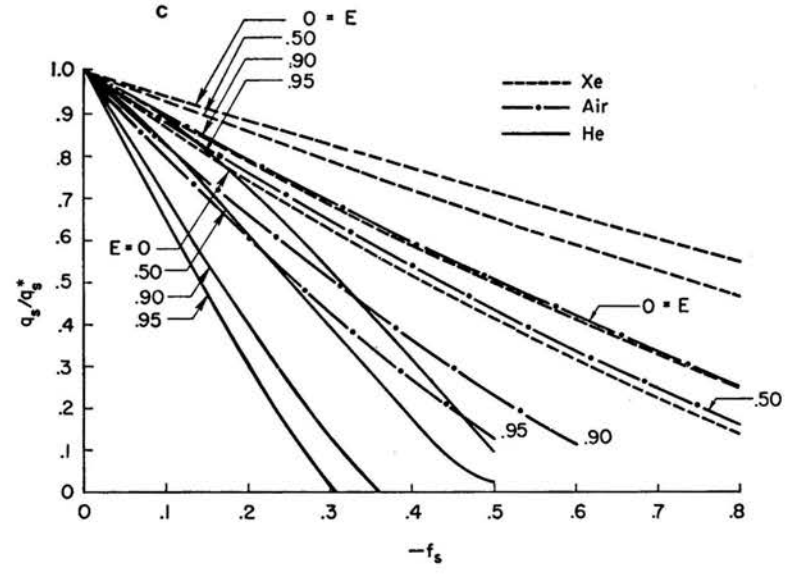

FIG. 5c. Effect of Mach number on heat transfer rate. $\beta = 0$, $g_s^* = 0.1$.

Newtonian flow gives $E = \cos^2\theta_c$, where θ_c is the cone half-angle. For convenience, we follow common practice and refer to the effects of E as Mach number effects. Figures 5a, 5b and 5c show the effect of Mach number on shear stress, mass transfer conductance and heat transfer rate for $\beta = 0$ and $g_s^* = 0.1$. Mach number effects at $g_s^* = 0.5$ and 0.9 can be evaluated by cross-plotting data from Figs. 3 and 4.

(i) Wall shear stress: Figures 3a and 5a bear a striking resemblance which is readily explained. The primary effect of increasing E is to decrease the free stream static enthalpy;

for $h_e = (1-E)H_e$, and H_e is not a parameter of the problem. Thus increasing E leads directly to a decrease in C_s, and gives an effect similar to that of increasing the wall temperature. For air injection the interlocked effect of E and g_s^* is easily seen for then we have the simple relation $C_s = [(1-E)/g_s]^{1/2}$. On the other hand, E and g_s^* do have a markedly different influence on the profile of C across the boundary layer. The viscous dissipation present for non-zero E has its distinctive effect on the temperature and hence the C profiles; for $\beta \neq 0$, compressibility plays a role as well.

The above observations suggest that the effects of both E and g_s could be correlated by modifying the injection parameter $-f_s$ with some function of C_s. Correlation schemes involving C in some manner have been used by a number of authors; for example, in Refs. 2 and 4, $C^{-1/2}$ evaluated for the free stream species at the Eckert reference temperature was included in the injection parameter. But as GROSS *et al.* [2] note, this approach is hindered in that the recovery factor with foreign gas injection is required for the calculation of the reference temperature. Such recovery factor data is sparse, and unreliable owing to its sensitivity to diffusional conduction and hence the thermal diffusion factor α_T. SIMON *et al.* [4] bypass the problem by approximating the recovery factor with its impermeable wall value.

(ii) Mass transfer conductance: Figs. 3b and 5b bear the same resemblance as was noted above for the shear stress. Similar comments on the role of C_s apply here as well.

(iii) Heat transfer rate: Turning now to the heat transfer, the situation is found to be more complex. The properties effects noted for shear stress are present and cause Figs. 3c and 5c to have some resemblence. But there is an additional consideration of an appropriate driving force for heat transfer with foreign gas injection and $E > 0$. The anomalous behavior of the heat transfer for $E = 0.9$ shown in Fig. 4c illustrates the problem. Figure 4c shows q_s/q_s^* at $g_s^* = 0.9$ for air injection only; for He and Xe values appreciably greater than unity obtain. The reason for the apparent reversal in behavior as g_s^* increases from 0.5 to 0.9 can be seen in Fig. 6, where $q_s = C_s g_s'/\mathrm{Pr}_s$ is plotted. For $g_s^* = 0.9$, the conductive

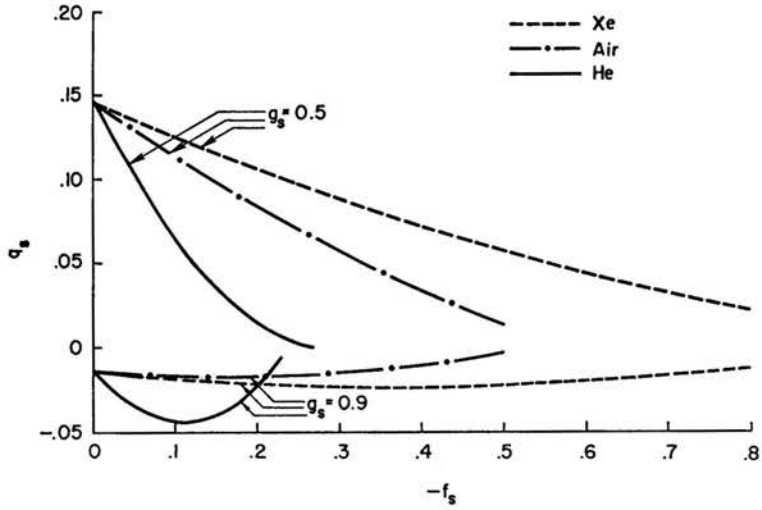

FIG. 6. Heat transfer rate. $\beta = 0$, $E = 0.9$.

heat flux is directed away from the wall, since the wall temparature is now higher than the recovery temperature. The variation of q_s with f_s does however retain its gross characteristic features; for example, boundary layer blow-off for the three injectants dictates the values of f_s at which q_s tends to zero.

In order for the heat transfer conductance to have an acceptable limiting behavior for the adiabatic wall situation it should be defined as $g_h = q_s/C_{pe}(T_r - T_s)$, where T_r is the recovery temperature including the effects of viscous dissipation, and for foreign gas injection the effects of diffusional conduction as well. For $E = 0$ and $\alpha_T = 0$, the definition reduces to $g_h = q_s/(h_e - h_{es})$. As already mentioned, data are sparse for the recovery factor $r \equiv (T_r - T_e)/(u_e^2/2C_{pe})$ with foreign gas injection. But there is a more fundamental question. The main interest in high Mach number flows with foreign gas injection lies in applications such as transpiration and ablative cooling, where the wall temperature is much less than the recovery temperature. Thus it does not seem wise to attempt to present cold wall data, on which diffusional conduction has negligible effect, in terms of a conductance based on recovery temperature, which in contrast is so dependent on this phenomenon. A similar dilemma is encountered when heat transfer data for high temperature air must be correlated; CHAPMAN [20], in his detailed study of heat transfer to cones in high speed air flow, did not calculate recovery temperatures and correlated his data in terms of C_s. No attempt will be made here to remove anomalies of the kind described in the preceding paragraph by introducing an approrpiate driving force.

3.5. Profiles

The velocity profiles depicted in Fig. 7a are representative of those calculated in the present study. Injection of helium results in velocity overshoots which become more marked with increasing wall to total temperature ratio. Conversely, injection of heavy gases decreases the wall velocity gradient. It should be noted that use of the transformed coordinate η as abscissa in Figs. 7 gives a distorted view of physical reality because the coordinate η is proportional to the integral of the local mixture density. When the concentration of injected gas near the wall is high (as is seen to be the case in Fig. 7b), the transformed coordinate for light gas injection is scaled down considerably relative to the physical coordinate; the opposite holds true for heavy gas injection. This is the reason for the apparently anomalous result that the boundary layer with helium injection is thinner than the one with an identical rate of xenon injection; in physical coordinates the opposite is true.

The concentration profiles shown in Fig. 7b show that for the same injection rate, the wall concentration of helium is higher than that of xenon. This feature is due to the relatively high rate of injection; although the diffusion coefficient of helium in air is much larger than that of xenon, the Schmidt number near the wall is much lower for helium in this case owing to the very low mixture density. At low rates of injection, for which $m_{1,s}$ is low, the trend is reversed and the value of $m_{1,s}$ for helium is lower than the xenon value for the same rate of injection. Again there is the apparent anomaly that the concentration boundary layer for helium appears thinner than that for xenon; in physical coordinates the reverse is true.

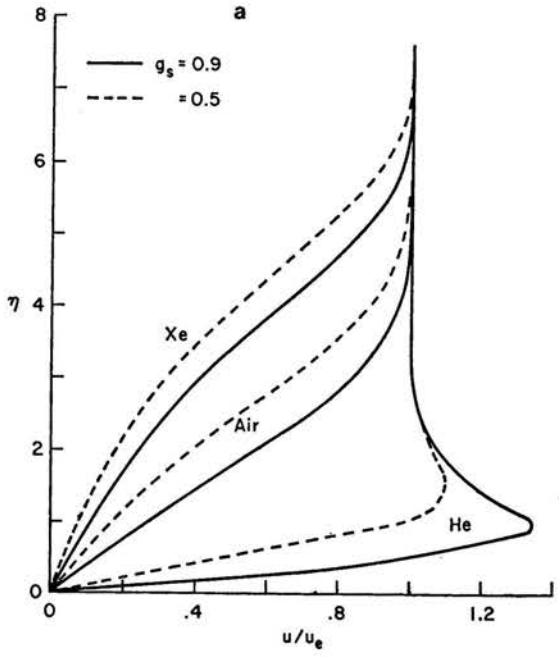

FIG. 7a. Velocity profiles. $\beta = 0.25$, $E = 0.5$, $f_s = -1.0$.

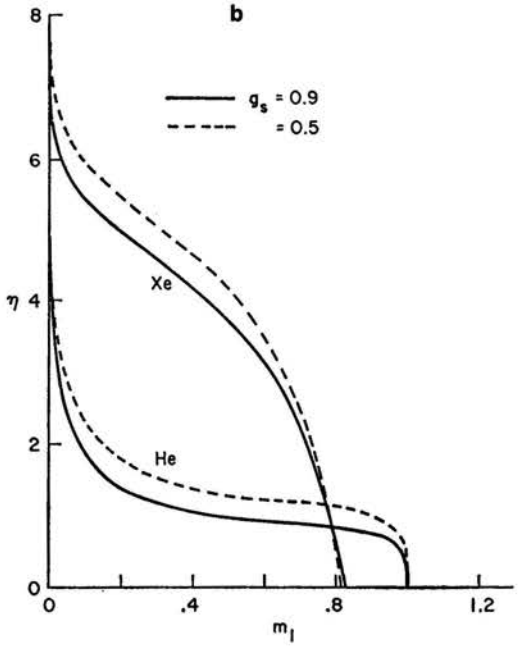

FIG. 7b. Concentration profiles. $\beta = 0.25$, $E = 0.5$, $f_s = -1.0$.

References

1. J. R. BARON, *The Binary-Mixture Boundary Layer Association with Mass Transfer Cooling at High Speeds*, M.I.T., Naval Supersonic Laboratory, Tech. Report 190, 1956.
2. J. F. GROSS, J. P. HARTNETT, D. J. MASSON, and C. GAZLEY, Jr., *A review of binary laminar boundary layer characteristics*, Int. J. Heat Mass Transfer, **3**, 198–221, 1961.
3. C. S. LIU, J. P. HARTNETT, and H. A. SIMON, *Mass transfer cooling of laminar boundary layers with hydrogen injected into nitrogen and carbon dioxide free streams*, Third International Heat Transfer Conference, Paper No. 83, Chicago, August 1966.
4. H. A. SIMON, J. P. HARTNETT, and C. S. LIU, *Transpiration cooling correlations for air and non-air free streams*, AIAA Paper No. 68–758, presented at the AIAA 3rd Thermophysics Conference, Los Angeles, June 1968.
5. E. M. SPARROW, W. J. MINKOWYCZ, and E. R. G. ECKERT, *Diffusion-thermo effects in stagnation-point flow of air with injection of gases of various molecular weights into the boundary layer*, AIAA Journal, **2**, 652–659, 1964.
6. P. A. LIBBY, and P. SEPRI, *Stagnation point flow with complex composition*, Phys. Fluids, **11**, 1621–1627, 1968.
7. N. A. ANFIMOV, *Heat and Mass Transfer near the Stagnation point with the injection and suction of various gases through the body surface*, Mekhanika Zhidkosti i Gaza, **1**, 22–31, 1966.
8. A. V. GOMEZ, A. F. MILLS, and D. M. CURRY, *Correlations of heat and mass transfer for the stagnation region of a reentry vehicle with multicomponent mass addition*, Space Systems and Thermal Technology for the 70's, Part II, ASME, June 1970.
9. A. F. MILLS, and A. WORTMAN, *Two-Dimensional stagnation point flows of binary mixtures*, Int. J. Heat Transfer, **15**, 969–987, 1972.
10. N. A. JAFFE, R. C. LIND and A. M. O. SMITH, *Solution to the binary diffusion laminar boundary-layer equations with second-order transverse curvature*, AIAA Journal, **5**, 1563–1569, 1967.
11. R. M. KENDALL, and E. P. BARTLETT, *Nonsimilar solution of the multicomponent laminar boundary layer by an integral matrix method*, AIAA Journal, **6**, 1089–1097, 1968.
12. V. E. DENNY, and R. J. KOCHAN, *Downstream effects of discontinuous injection of foreign gases in inert laminar boundary layer flows*, Proceedings of the 1972 Heat Transfer and Fluid Mechanics Institute (R. B. LANDIS and G. J. HORDEMANN, ed.), Stanford University Press, 1972.
13. J. R. BARON, *Thermal diffusion effects in mass transfer*, Int. J. Heat Mass Transfer, **6**, 1025–1033, 1963.
14. L. LEES, *Laminar heat transfer over blunt-nosed bodies at hypersonic flight speeds*, Jet Propulsion, **26**, 259–269, 1956.
15. J. O. HIRSCHFELDER, C. F. CURTISS, and R. B. BIRD, *Molecular theory of gases and liquids*, 2nd ed. John Wiley, New York 1964.
16. R. A. SVHELA, *Estimated viscosities and thermal conductivities of gases at high temperatures*, NASA TR R–132, 1962.
17. E. T. DERGAZARIAN, *et al.*, *JANAF thermochemical tables*, The Dow Chemical Co., Midland, Mich., Dec. 1960, and supplements to date.
18. A. WORTMAN, *Mass transfer in self-similar laminar boundary-layer flows*, Ph. D. Dissertation, School of Engineering and Applied Science, University of California, Los Angeles 1969.
19. A. WORTMAN, and A. F. MILLS, *Highly accelerated compressible laminar boundary-layer flows with mass transfer*, J. of Heat Transfer, **93**, 3, 281–289, 1971.
20. G. T. CHAPMAN, *Theoretical laminar convective heat transfer and boundary-layer characteristics on cones at speeds up to* 25 km/sec, NASA TN D-2463, 1964.

AERODYNAMICS RESEARCH BRANCH, AIRCRAFT DIVISION,
NORTHROP CORPORATION HAWTHORNE, CALIFORNIA
and
UNIVERSITY OF CALIFORNIA, LOS ANGELES